# Investigation on the fuel distribution in DI Diesel engine combustion chambers and its influence on soot emission

Prof. Dr.-Ing. Berthold Grünwald, guest professor, Technische Hochschule Darmstadt
Dipl.-Ing. Heinz-W. Kuhnt, research assistant, Technische Hochschule Darmstadt
Dr.-Ing. Victor Gheorghiu, guest scientist, Technische Hochschule Darmstadt

## Abstract

This report is a summary of all the work done during the lost year in the field of mixture formation in Diesel engines. The work was performed in the department of combustion engines at the Technische Hochschule Darmstadt (Head: Prof. Dr.-Ing. G. Hohenberg). The subsequent report consists of three parts. In the first part a model of an injection jet is formed, where the structure of the jet consists of vapor, air and droplets. Concentrations of droplets and vapor are varying over a cross-section of the trajectory in such a way, that in the centerline the maximum value occurs and at the boundary the value is zero.

The model is taking into consideration a statistical distribution of the droplet diameter: In each cross section of the jet k species of droplets are located with varying diameters in the range of a minimum and a maximum value. The jet movement is calculated considering the influences of initial impulse, swirl and squish flow of the cylinder mass and the flow resistances.

In the second part of this paper the model is applied on a direct injection Diesel engine which was motored stationary and transient. It is possible to show, that in a transient test procedure the process of fuel distribution on the piston wall and evaporation in the jet is varying.

In the third part of this report is shown, that there is a connection between the process in the interior of the engine, i.e. mixture formation and combustion on one side and the soot emission on the other side. It is possible to prove, that the free mass of fuel vapor, which is formed during the ignition delay period, has a very important influence on the soot emission. The free mass of vapor affects the first period of combustion and thus the velocity of the soot formation reaction. Based on stationary and instationary engine tests a soot index was developed, which demonstrates many important influences of the running conditions. Therefore, it is possible to show, that, by use of the soot index, the various influences, like engine speed, vapor mass, air-fuel-ratio and other terms can be well described.

# 1. Introduction

In DI-Diesel engines the fuel is distributed in the air and on the piston wall [1], [2]. In both cases, the process of vaporization and mixture formation is quite different [3], [4]. At the beginning of the studies, a model of a fuel jet was developed to get information about the following processes:

1: The movement of the fuel jet in the cylinder under influence of air swirl and squish.

2: The wetting of the piston wall by the fuel. The main interest concerns the temperature of the fuel droplets, the area where the droplets hit the wall and the quantity of fuel on the wall.

3: The progress of heating and vaporization of the droplets inside a fuel jet.

This newly developed model was used to analyze, if the fuel distribution in the cylinder and the ratio between fuel distributed in air and on the wall, is very much different in stationary and instationary operation. It is also interesting to get information, whether these differences cause significant changes in the combustion process and the emission of soot. In the instationary operation, several processes are expected to be clearly variable like the spray formation, the spreading of the jet, air movement, droplet heat-up and vaporization.

# 2. Model of the fuel jet

The jet model is based on newer experiments. Well known are models, in which the jet is regarded as a system of gas [5]. These models have been already used for the analysis of jet streams in the combustion chambers of DI-Diesel Engines [6], [7]. Newer results with the RAMAN spectroscopy [8] [9] show the presence of fuel droplets even in a large distance from the injection nozzle (figure 1), and so an improved, sophisticated spray model is necessary. The essential velocities and coordinates, which are used for this model, were defined in accordance with figure 2.
In consideration of these results a model of an inhomogeneous multi-phase jet was developed, where the jet consists of a gaseous mixture (fuel and air) and fuel droplets (figure 3 a, b).
The structure of the jet is defined as follows:

a) In a cross-section with radius $r_j$ are three main variables, the velocity *w*, the concentration of fuel C and the mass flux of the droplets or liquid fuel *y*. All these variables differ in the whole cross-section. All notations with the index *m* refer to the centerline of the jet. The equations for the distribution of velocity and concentration were presented by ABRAMOVITSCH and JOHNSTON [6], [7] (figure 3, eq. 3-1...3-3). According to these equations, the maximum of velocity and fuel concentration can be found in the centerline of the jet.
b) The maximum fuel concentration is on the axis and thus, there is the lowest air-fuel ratio. The surrounding air is entering the jet axial and transversal. So, the concentration decreases from the middle to the border of the jet, where the concentration equals zero.

c) The mass flux of the liquid fuel decreases the maximum in accordance with an exponential equation. With the experimental results (shown in figure 3) an equation for the calculation was developed (eq. 3-4). The flow of the droplets, related to a standard value of a plane, is determined by equation 3-5, where $m_D$ relates to all droplets of the same species, that means with the same diameter.
d) The distribution of the droplet diameter is supposed to be statistical. This function is approximated step by step, so that *k* species of droplet diameters occur, that means, that this function has to be calculated for each individual cross section. The arithmetical value of the droplet diameter $d_{Dm}$ is defined as a function of the injection nozzle geometry, the physical data of fuel and the density in the cylinder (figure 3 eq. 3-6, [3]). The proposed distribution is equivalent to an exponential equation (figure 3 d, eq. 3-7, 3-8) and the coefficients and the probability $p_m$ are based on experimental data [10].
e) The jet motion is calculated beginning with its impulse when entering the combustion chamber under consideration of swirl ($\omega$), velocity of squish ($w_Q$) in the combustion chamber and flow resistance ($c_D$) (figure 2).

# 3. Differential equation system for jet and evaporation

## 3.1 Conservation of droplet number among the jet

The number of droplets of one species *k* in the jet is considered as constant until vaporization. So the frequency of the droplets in a cross section with the radius $r_j$ is constant, too. With this proposition and under consideration of the droplet distribution in the jet, it comes to equation (1). All notations with the index *o* specify the conditions in the initial cross-section of the jet. This cross-section is not found at the injection nozzle directly, because the injection jet is fully developed in a distance from the nozzle. Replacing the variable $y_k$ and the radius *r* in equation (1) with the equation (3-3) and (3-4) results in eq. (2).
If $m_{Dk} = 0$, the mass flux $y_{m,k}$ becomes zero, too. This means, that eq. (2) is valid until the end of vaporization. The equation (2) is a conservation law and shows that the difference of the droplet number between two jet sections equals zero and this results in equation (3).

## 3.2 Mass conservation in the jet

The conservation law shows the constancy of the fuel mass of the droplets with the species *k*, if the droplet moves through a section of the jet with the elongation *ds*. The total differential of the mass disappears and this results in eq. (4). The first part of this equation describes the rate of droplet vaporization (eq. (5)). By differentiation of equation (3) with the coordinate *s* and the use of equation (5) the conservation of droplet mass for the species *k* in the jet element *ds* (eq. (6)) is obtained.

### 3.3 Balance of vapor mass

In the mixture of fuel vapor and air the fuel is present in a concentration *C*. This concentration varies throughout the cross-section as shown in figure 3. The total mass flow in a jet segment can be calculated by eq. (7). The density $\rho_m$ is calculated as the density of an ideal gas mixture consisting of fuel and air. In the interval *ds*, the increasing of the vapor mass, which is a part of the mixture, is proportional to the changing of the vaporization rate (eq. (8)). By inserting the values *C*, *w* (from figure 3) and $\rho_m$ the equation (9) is formed. In order to solve equation (9), another equation for $\partial(\dot{m}_v)/\partial s$ is necessary. Furthermore it is to be considered, that between two cross-sections a certain amount of vapor was generated. The droplet frequency $f_k$ for the species *k* in a jet section is calculated by equation (10). On the other hand, the mass of a droplet in a unit of length can be defined by (11).
Hence, for the variation of the vaporization rate in the interval *ds* the equation (12) is valid. With the fact, that all species respond to the same distribution function, one gets the equation (13). By adding the vapor mass of all species, we obtain the equation (14). At least the balance of the vapor (eq. (15)) is formed by equation (14) with equation (9).

### 3.4 Balance of the fuel-air- mixture

The total mass flow in the injection jet consists of the components fuel and air. In order to calculate the mass flow variations along the jet centerline, the variations of all the individual components is to be considered (eq. (16)). Assuming, that the air enters the jet area as well axially as perpendicularly to the jet direction, we obtain (according to [5]) equation (17). The coefficients $\alpha'$ and $\beta'$ are corrected according to the publications [5], [6], [7]. After inserting the velocity *w* from eq. 3-1 and the density $\rho_m$ into equation (16), the equation (18) is received.

### 3.5 Impulse equation

The derivation to the coordinate *s* is projected to the coordinate *x* (eq. (19)). The differential equation to the other coordinates are formed in a similar way by substituting *x* by *y* and *z*. All terms with the trigonometric functions describe a fraction of the velocity vectors in direction of the coordinates *x*, *y*, *z*. The notation $I_{ij}$ means an abbreviation, which is explained in the notation chapter. The density $\rho_m$ means the density in the jet.

### 3.6 Differential equation for the droplet vaporization

As a first step, a free droplet shall be regarded, which is in resting position and homogeneous regards the chemical composition and temperature. In the following steps, a movement of the droplets, which is relative to the air and the reciprocation of the droplets among themselves will be introduced. The vaporization proceeds only under instationary conditions. Thus the droplet temperature is increasing continually from $50°C$ to the critical temperature.

### *3.6.1 Heat-balance of a droplet*

With the heat balance of the droplet (eq. (20)) it is possible to get the droplet temperature. Equation (21) results from [11] and [12]. According to [13], the gradient of droplet temperature (eq. (22)) is received.

### *3.6.2 Changes of the droplet density*

The droplet mass balance expresses the influence of the droplet temperature on the density of fuel $\rho_D$ and so it is possible to receive eq. (23). The derivation of $\rho_D$ can be calculated with the function $\rho_D(T)$.

### *3.6.3 Mass transfer*

The vapor diffusion from the surface of the droplet to the surroundings can be calculated by the law of FICK (eq. (24)). The vapor pressure has been determined by the equations of CLAPEYRON, of LEE and KESSLER and of WAGNER. All these equations have already been presented in [14]. The diffusion coefficient was taken from WILKE and LEE [14] and BIRDE [15], [16]. The calculation of the density is a method by RACKETT and HANKINSON-THOMSON [14]. All other properties of the fuel and the air are basing on data, taken from the literature [17] ... [23].

In a Diesel jet, a droplet can vaporize completely or partly. The droplets diameters in the jet are distributed statistically and it is to assume, the smaller droplets vaporize so quickly, that they cannot reach the piston wall. It mainly depends on the temperature of the cylinder mass if the smaller droplets heat up to the critical temperature. For example: Tetradecan has the critical values $T_k = 653K$ and $p_k = 14.4bar$. In this case, the droplet converts into a mass of vapor with high density, before the droplet diameter has reached the values zero.

Since no further knowledge exists so far and with respect to the fact, that a small fraction of a droplet reaches the critical temperature, it is to assume, that the mass transfer from the vapor core to the surrounding air takes place at critical temperature.

The biggest droplets may not heat up and vaporize completely and that is the reason, why they hit the piston wall. The heat-up procedure reaches a droplet temperature, which is not as high as in the critical state; however in certain cases the temperature can be higher than the piston temperature. This has the consequence that those droplets cannot get sufficient energy for the vaporization from the piston wall.

*3.6.4 Correction of heat- and mass transfer coefficients*

Several calculation models are known for a free uninfluenced droplet. In the injection jet another situation is existent, because the droplets are influencing each other and are also influenced by the gas flow, which is not known exactly.

One possibility to describe the droplet movement is to use a simpler model and to correct it by the RANZ-MARSHAL method [24] ... [26]. After introducing this correction, the diffusion coefficient *D* and the heat transfer coefficient *h* can be calculated by equation (25 a, b). With the use of this correction, two problems occur: 1. How big is the representative flow velocity for the REYNOLDS number? 2. What is the value for the constant *c*?

If this calculation is based on an average velocity of jet and air in the cylinder and fixed constant $c = 0.3$, as it was recommended by RANZ-MARSHAL, this will result in very high correction values. That was the reason, why the authors chose $c << 0.3$.

# 4. Computer program

For the described jet model a simulation program has been developed and thus it was possible to make up a correlation between jet model and experiment. The numerical integration of the differential equations was realized with RUNGE-KUTTA method of fourth order. The calculation of the material data as vapor pressure, enthalpy, density, diffusion coefficient and so on, encloses mainly the dependence from pressure and temperature. The graphic section of the program produces evident presentations of droplet diameter distribution, jet tracks and droplet temperature. For the simplification of the program, the jet is divided in several parts jets.

Beside this, the injection process is separated into single segments, witch are following each other. For each interval $\Delta\alpha$ ($\Delta\alpha$ was fixed to $1°CA$) the number of injection intervals is $j = \Delta\alpha_{EZ} / \Delta\alpha$. Hence each jet section a mean diameter of the droplets is calculated and also a statistical distribution of this diameter. Each section of the jet is treated separately, and its motion and vaporization are obtained for an integral of $\Delta\alpha = 0.25°CA$.

# 5. Calibration of the constants

The fuel is considered as a one-component-system in this model. The material data correspond to those of Tetradecan. The system of the differential equations includes four constants. These constants have been calculated by a method, which has been presented in [6], [7]. Besides, a comparison with the measurements of CHIU [27] has been carried out. On this basis, the following values have been fixed: $\alpha' = 0.01$; $\beta' = 0.02$; $c_D = 0.1$. For the constant *c* a value of $c = 0.021$ was found. This value significantly deviates from the constant, which RANZ-MARSHALL have proposed for the condition of free droplets: $c = 0.276$. The difference in this constant show, that

the conditions in the combustion chamber are not comparable to a free droplet. It can be assumed, that the reciprocation of the droplets and vapor are influenced by pressure, temperature and relative velocity between air in cylinder and injection jet. Besides all, the process has been treated as a global process. Thus, the conclusions about the conditions of a single droplet are very difficult.

# 6. Engine testing

The approval of this newly developed model was made by stationary and transient motor tests. Two different engines have been used, which are comparable in terms of the geometrical data (table 1). The stationary tests have mostly been realized with the 1-cylinder engine. All the transient testing took place with the 6-cylinder engine. For the transient testing, acceleration was simulated as it occurs during a start at a traffic light. The most important results of middle speed data acquisition are shown in figure 4 a, b. In a time of 4 seconds, the whole range of engine speed is driven through.

Within the first two seconds, a distinct soot peak occurs and this happens coincidentally with the lower engine speed. With increasing speed, the soot emission considerably reduces. Since the speed is increasing quickly, the air consumption increases too.

As a result, the boost pressure does not become higher though the turbocharger speed increases in the first period of the acceleration. The central question was: what happens in the combustion chamber in the period when the high soot emission occurs? To get information about this, all the cycles have been recorded (figure 5). The analysis of these measurements shows that after two seconds a nearly constant mean indicated pressure is obtained but the maximum pressure increases further on. In the first period of the acceleration, significant changes in ignition delay time and combustion process occur in comparison to the stationary testing.

The position of maximum pressure and maximum temperature deviates perceptible from each other. An other remarkable phenomenon is shown in the graphs of the heat release maximum and the position of this maximum (figure 5). An impression of the changes in the engine process during transient tests is obtained by figure 6. One remarks a shifting of the fuel amount burned in the first phase of combustion to the second phase. Also impressive are the differences of the heat release in comparison to the stationary mode.

Very important deviations are shown in the mixture formation process. For direct comparison three cycles have been selected, the heat release graphs of which are shown in figure 6. A comparison of the injection jets is shown in figure 7. The swirl of these cycles is shown in figure 8. With these figures, it is possible to get following results:

Regarding all injection jets it is to be seen that a part of the fuel reaches the piston wall. Because of the excentrical position of the injection nozzle four jets with different length occur. This causes a significant difference in the amount of fuel on the piston wall, as shown in figure 10. The mass of al jets adds up to *31* percent of the total

mass in the case of full load operation. *80* percent of these *31* percent reach the wall in the short jets, i.e. also the long jets participate in the touching of piston wall. Likewise the figure shows, that the tracks on the wall are much smaller than those in the case of the short jets.

One remarks that just at a speed of *1100 1/min* (instationary mode) the injection jets have an intensive contact with the wall. The situation is completely different in stationary operation and at higher speed. There is to remark a significantly increased drifting of the jet, witch is mainly caused by the swirl in the combustion chamber (figure 8). In figure 9 the phenomena in the jet are shown more detailed. The left side shows the droplet distribution near the nozzle. The middle part shows the distribution on the wall. Caused by the higher engine speed, the injection process in the cycle shown in figure 9c prolongs by nearly *6°CA*. In general, it is to find out that the droplets partly vaporize and also extended because of the increasing temperature. In the middle part of these figures, one can see that at *1000 1/min* (instationary mode) droplets of the species 4 and at *1960 1/min* (instationary mode) only droplets of species 5 and higher reach the wall. Taking into account the results of figure 7, it is to conclude from the calculations, that at the higher speed and with stationary operation the droplets are spreaded over a large surface.

Since the droplet diameters are smaller in the stationary point and at high engine speed, the probability that a complete fuel film is formed is less.

Under the point of view, that film evaporation on the wall is important, it is also interesting to know the droplet temperatures when they reach the piston wall. It is remarkable that the mean temperature of each section of jet no. 2 is higher than the temperature of jet no. 1. In jet no. 2 and no. 3 the mean temperature of the total amount of fluid fuel which reaches the wall is nearly *100°C* higher than in the short jets (table 2a). The consequence of this fact is a significant changing of the evaporation rate, witch is also proven by the values of vapor pressure shown in table 2b. It is perceptible that the vapor pressure in the longer jets is twice or three times higher than in the short jets. Furthermore it can be expected, that the vaporization process on the piston wall is proceeding more slowly. Later it will be demonstrated, that this can affect the soot emission of the diesel engine. If we compare the droplet temperatures for all the cycles when the jets hit the wall, they can recognize a clear difference (figure 9a-c). These temperatures deviate from each other regarding all the cycles. It is to conclude, that the heat-up of the droplets at the beginning of the acceleration is smaller than in the stationary operation.

# 7. Influence of vaporization on the exhaust soot concentration

Rich flames producing soot appear usually in diesel engines. The highest value of soot concentration is found around the TDC, namely $2000 - 3000 \cdot mg / Nm^3$. Such a concentration represents about $2 - 4\%$ of the fuel quantity per cycle. The concentration of carbon in the exhaust gas represents only $1 - 3\%$ of the highest concentration in the cylinder. KAHN evaluated in 1969 (according to [28]) that the

soot formation in the combustion chamber is more important that the soot oxidation. Later (1980) HIROYASU et. al. [28] paid more attention to the soot oxidation.

Subsequent investigations [2], [29], [30] indicated, that soot is created right from the beginning of combustion and reaches is maximum value in the first part of combustion. In the second stage of combustion soot concentration decreases and the chemical reaction of soot formation seams to "freeze" at the end of combustion. According to [2] the main amount of soot - about *55*% - is yielded in the diffusion flame (by droplet combustion), about *30*% of soot is formed through the combustion of fuel film on the wall (piston bowl). Only a small quantity of soot is built in a premixed flame. According to [29], soot concentration is $10000 \cdot mg/Nm^3$ at the edge of the piston bowl, and that is obviously much more than the soot concentration near by nozzle orifice ($3000 \cdot mg/Nm^3$). All these results indicate two essential actions, namely: 1. the soot formation is strongly intensified around the TDC, 2. a strong intensification of the soot oxidation process during the second part of combustion.

Starting from these observations it is possible to show, that fuel vaporization has a great significance concerning the soot formation rate $\dot{m}_S$ and the soot oxidation rate $\dot{m}_{Ox}$. It was assumed that soot formation and soot oxidation are taking place simultaneously. The soot mass at the end of expansion stroke $m_{SE}$ will be calculated by equation (26). According to [30] $\dot{m}_S$ and $\dot{m}_{Ox}$ may be determined by equation (27a,b), where $m_{vf}$ is the free vapor mass in cylinder. The constants $K_S$ and $K_{Ox}$ are determined only by pressure and temperature.

The free vapor mass will be calculated in terms of a mass balance equation (eq. (28)) where $m_v$ is the total mass of vapor, the formation of witch starts at the beginning of the injection up to a fixed crank angle $\alpha$, and $m_b$ is the total amount of burned fuel. The variable $m_b$ is determined in dependence of the course of the heat release. Equation (28) shows a correlation between soot formation, mixture formation and heat release. The mass $m_v$ gets calculated on the basis of a vaporization model in a spray. Thus it becomes possible to calculate the mass $m_{vf}$, what is essential to solve equation (27a). Every engine has an optimum value for the theoretical swirl ratio $\omega_{opt}$ at a fixed engine speed, when the soot emission reaches a minimum. However the effective swirl ratio $\omega$ is caused by constructive features. That is one reason why the authors propose a correction factor f (eq. (29)) to take into account the deviation of $\omega$ from the optimum value $\omega_{opt}$.

By substituting $\dot{m}_S$, $\dot{m}_{Ox}$ in (26) with the values of equation (27a,b), and the time $t$ by the crank angle $\alpha$ the equation (30) will be obtained. In this equation $I_S$ and $I_{Ox}$ are abbreviations of the two integrals (eq. 31a,b). The present stage of knowledge does not allow determining acceptable values for the constants $A_S$ and $A_{Ox}$ in equation (30). That is the reason, why it is doubtful to use the equation (30) to calculate soot emissions. Nevertheless the authors have made an attempt to obtain an index of particulate emissions in terms of equation (30). Thus they developed a criterion presented in equation (32), where for the sake of simplification the variable $m_{vf}$ was

replaced by a constant value $m_{vflD}$. This value describes the free vapor mass at the end of ignition delay time. At least in order to express clearly the influences of different parameters the substitution $m_{vflD} = R_{vlD} \cdot m_f$ have been used, where $m_f$ is the fuel quantity per cycle and $R_{vlD}$ appears as a fraction of $m_f$. One can observe that the smaller the soot index the smaller becomes the soot emission.

Although the soot criterion offers a strong simplification of a very complicated reality, we can emphasize several influences of some parameters concerning the particulate emissions. For example there is an explicit influence of the engine speed, namely when $n$ increases $K_{SE}$ decreases and at the same time the soot emission is diminishing. On the other hand, simultaneously with the engine speed other factors increase like the correction factor $f$, ignition delay and free vapor mass change as a result of changes in spray velocity, droplet diameters, droplet heat-up and vaporization. By the way, the influence of engine speed becomes very complex and it is difficult to explain simply the tendency of soot emission modification.

The soot index $K_{SE}$ has been calculated for many thermal cycles. Its value has been compared with the soot concentration measurements in the exhaust gas. The comparison indicates that the variation tendency of the soot index and the concentration is the same (figure 11). If we compare the full load cycles No. 19 (stationary running) and No. 52 (acceleration running) we find out, that the mixture formation in both cycles is very different (figure 9). For example the free vapor mass $m_{vflD}$ is by *50*% smaller in the cycle No. 19. As a result $K_{SE}$ is smaller and in the same proportion the soot concentration decreases. The same results have been achieved by use of stationary cycles as shown in table 3. In these results from an injection advance variation one can also see the clear dependence between soot index, smoke number and injection advance.

# 8. Conclusions

The correlation between soot emission and free vapor mass indicates the significance of the calculation of the evaporation process. In a simplified manner it is possible to substitute the course of the free vapor mass $m_{vf}$ by a constant value, namely the free vapor mass at the end of ignition delay time $m_{vflD}$. If we want to calculate $m_{vf}$ or even $m_{vflD}$ we have to calculate simultaneously the fuel distribution in the combustion chamber since the vaporization rate different values in the air or on the wall (on the piston bowl). In accordance with this research, the fuel distribution in the combustion chamber and the course of vaporization are subject to strong alterations in an acceleration process from cycle to cycle [31].

It remains a task for future investigations to find out what kind of possibilities are being offered by the improvement of the mixture formation (using modified values of squish and swirl rate of air) during the acceleration process with view to lower soot concentration. On the other hand, it should be interesting to know if it is possible to improve the vaporization calculus taking into account that fuel droplets are multicomponent systems [32].

# 9. References


[1] Breuer, B.: Über die Wandberührung von Kraftstoff im schnellaufenden Dieselmotor mit direkter Einspritzung, Diss. RWTH Aachen, 1970, (page 2)

[2] Norris-Jones, S. R.: A Study of the Formation of Particulates in the Cylinder of a Direct Injection Diesel Engine, SAE-Paper 840419, (page 2,8)

[3] Müller, E.: Gemischbildung im Dieselmotor bei Kraftstoffwandanlagerung, Diss. TH Darmstadt, 1976, (page 2, 3)

[4] Ramos, J.I.: Internal Combustion Engine Modeling, Hemisphere Publishing Corporation, 1989, (page 2)

[5] Ricou, F. P., Spatding, D. B.: Measurements of entrainment by axi-symmetric turbulent jets, J. Fluid Mech, 1961, 9, (page 2,4)

[6] Apostolescu N. et. al. : Fuel Spray Model for the Mixing Process Analysls in Combustion Engines, Rev. Roum. Sc. Techn., Electr. et Energ, 1983, 1

[7] Apostolescu, N. et ai. : General Fuel Spray Mode[ for the Mixing Process Analysis in Combustion Engines, Rev. Roum. Sc. Techn., Electr. et Energ, 1987, 2, (page 2,4,6)

[8] Knoche, K. F.,Heinze, Th.: Ramanspektroskopische Untersuchungen zur Gemischbildung in Einspritzstrahlen, B 224 "Motorische Verbrennung", RWTH Aachen, 1988, (page 2)

[9] Pischinger, F.: Grundtagen und Entwicklungslinien der dieselmotorischen Brennverfahren, VDI Berichte 714, 1988, (page 2)

[10] Grünwald, B, Kuhnt, H.-W., Lippert, D.: Berechnung der entzogenen Wärme und der Verdunstungsrate von Kraftstoffstrahlen in Dieselmotoren, Interner Bericht, Verbrennungskraftmaschinen, TH Darmstadt, 1989, (page 3)

[11] El Wakil, M. M., Uyehara, 0. A, Myers, P. S.: A Theoretical Investigation of the Heating-up Period of Injected Fuel Droplets Vaporizing in Air, NACA TN 3179, 1954, (page 5)

[12] El Wakil, M. M. et ai.: Experimental and Calculated Temperature and Mass Histories of Vaporizing Fuel Drops, NACA TN 3490, 1956, (page 5)

[13] Manrique, J. A. : Theory of Droplet Vaporization in the Region of the Thermodynamic Critical Point, NASA CR-72558, 1969, (page 5)

[14] Reid, R., Prausnitz, J., Poling, B.: The Properties of Gases and Liquids, McGraw-Hill, (page 5)

[15] Bird, R. B. et al.: Transport Phenomena, New York, 1960, (page 5)

[16] Mersmann, A.: Stoffübergang, Springer-Verlag, 1986, (page 5)

[17] Prausnitz, J. M, Chueh, P. L.: Computer Calculations for High-Pressure Vapor-Liquid Equilibria, Prentice-Halt, 1968, (page 5)

[18] Lefevbre, A. L.: Gas Turbine Combustion 9 - Gas Turbine Fuel, Hemisph. Publ. Corp., New York, (page 5)

[19] Waldmann, H., Seidel, G. H.: Kraft- und Schmierstoffe, Technischer Verlag Herbert Gram, Berlin, 1979, (page 5)

[20] * * * : VDI-Wärmeatlas, Dal-Da24, Dct-Dc2, 3. Auflage, 1977, (page 5)

[21] * * * : Arbeitsmappe für Mineralölingenieure, D2-D5, Jt-J7, VDI Verlag 1962, (page 5)

[22] * * * : Berechnung thermodynamischer Stoffwerte von Gasen und Flüssigkeiten, VEB-Verlag, 1966, (page 5)

[23] D'Ans, Lax: Taschenbuch für Chemiker und Physiker, Springer-Verlag 1964„ (page 5)

[24] Ranz, W. E, Marshalt, W. R.: Evaporation of Drops, Chem. Engng. Prog. 48, 1952, (page 5)

[25] Grübler, Erk, Grigul : Wärmeübertragung, Springer Verlag, 1963, (page 5)

[26] Prakash, S., Sirignano, W. A. : Theory of Convective Droplet Vaporization with unsteady Heat Transfer in the Circulating Liquid Phase, Int. J, Heat Mass Transfer, Vol 23, 1980, (page 5)

[27] Chiu, W. S., Shahed, S. M., Lyn, W. T. : A Transient Spray Mixing Model for Diesel Combustion, SAE No. 760128, (page 7)

[28] Hiroyasu, H., Akai, M., Nakanishi, K. : Soot Formation and Oxidation in Diesel Engines, SAE 800252, (page 8)

[29] Matsui, Y, Kamimoto, T., Matsuoka, S. : Formation and Oxidation Processes of Soot Particulates In D.I. Diesel Engine, SAE 820464, (page 8)

[30] Kano, S., Nagao, A., Motooka, H. : Prediction of In-Cylinder Flow and Spray Formation Effects on Combustion In Direct Injection Diesel Engines, SAE 850108, (page 8)

[31] Kuhnt, H.-W. : Untersuchung des Arbeitsprozesses und der Rußbildung beim Beschleunigungsvorgang von turboaufgeladenen Nfz-Dieselmotoren, Dissertation, TH Darmstadt, 1990, (page 10)

[32] Grünwald, B. : Tropfenmodelle für die Diesel- Einspritzung mit Mehrkomponentensystemen, Bericht der FG Verbrennungskraftmaschinen, TH Darmstadt, 1990, (page 10)

# 10. Notations

| | |
|---|---|
| $A_{ox}$ | constant, equation for soot-oxidation |
| $A_S$ | constant, equation for soot-formation |
| c | correction factor in RANZ-MARSHAL correlation |
| C | fuel concentration in spray |
| $c_D$ | aerodynamic drag coefficient |
| $c_{pv}$ | specific heat of vapor at constant pressure |
| $c_{pD}$ | specific heat of droplet at constant pressure |
| $d_o$ | nozzle hole diameter |
| $d_{max}$ | maximum diameter of droplet |
| $d_D$ | droplet diameter |
| $D_{fa}$ | diffusivity constant between fuel and air |
| $f_k$ | frequenzy of droplets |
| h | heat transfer coefficient |
| $I_{Ox}$ | integral of thermodynamic fraction in the soot-oxidation relation |
| $I_S$ | integral of thermodynamic fraction in the soot-formation relation |
| $K_{Ox}$ | thermodynamic fraction of soot-formation relation |
| $K_S$ | thermodynamic fraction of soot-oxidation relation |
| $K_{SE}$ | characteristic smoke number |
| L | spray penetration |
| $\dot{m}_v$ | mass flow rate of vapor |
| $m_v$ | vapor mass formed up to $\alpha$ °CA |
| $m_{vf}$ | free vapor mass |
| $m_{vf/ID}$ | free vapor mass, formed during the ignition delay time |
| $m_f$ | fuel mass per cycle |
| $\dot{m}_a$ | mass flow air |
| $\dot{m}_{ox}$ | soot-oxidation rate |
| $\dot{m}_S$ | soot-formation rate |
| $m_{SE}$ | soot-mass at the end of expansion stroke |
| $m_D$ | mass of droplet |
| $m_{Dv}$ | vapor mass formed by single droplet |
| $\dot{m}_{Dv}$ | evaporation rate of droplet |
| $m_{Do}$ | initial mass of droplet |
| $m_b$ | burned fuel up to $\alpha$ °CA |
| $M_f$ | molar mass of fuel |
| n | engine speed |
| p | cylinder pressure, probability |
| $p_m$ | maximum value of probability |
| $p_v$ | vapor pressure |
| $p_k$ | critical pressure |
| $p_{O_2}$ | partial pressure of oxygen |
| Pr | Pandtl number |
| Q | total heat tranfer from air to droplet |
| $Q_d$ | heat to heat up the liquid droplet |
| $Q_v$ | heat to vaporize the droplet |
| $Q_s$ | total heat transfer at the droplet sureface |
| $Q_{\Delta h}$ | heat tranfer to superheat the vapor |
| r | enthalpy of vaporization |
| $r_j$ | radius of spray cross section |
| $r_{jo}$ | initial radius of spray cross section |
| Re | Reynolds number |
| $R_f$ | gas constant of fuel vapor |
| $R_a$ | gas constant of air |
| s | length of the spray trajectory |
| Sc | Schmidt number |
| t | time |
| $t_{EE}$ | time at the end of expansion stroke |
| $t_{IA}$ | time of injection advance |
| $T_F$ | temperature, fuel film on piston wall |
| $T_c$ | critical temperature |
| T | temperature, gas in cylinder |
| $T_D$ | temperature of droplet |
| $T_{DA}$ | mean temperature of fuel and air |
| $R_{VID}$ | relative vapor mass up to burning advance |
| $w_o$ | fuel velocity at the nozzle hole |
| $w_a$ | tangential velocity of swirl |
| $w_m$ | maximum velocity in the spray |
| $w_{ma}$ | air velocity on jet centerline |
| $w_Q$ | velocity of squish motion |
| $y_k$ | mass flux of liquid fuel |

| | |
|---|---|
| $\alpha$ | crank angle |
| $\alpha'$ | axial entrainment coefficient of air |
| $\alpha_{IA}$ | injection advance |
| $\alpha_{IE}$ | injection end timing |
| $\alpha_{EE}$ | end of combustion |
| $\beta'$ | normal entrainment coefficient of air |
| $\Delta\alpha$ | computed interval |
| $\Delta\alpha_{ez}$ | injection time |
| $\varphi$ | angle between velocities $w_m$ and $w_a$ |
| $\lambda$ | air fuel ratio |
| $\lambda_u$ | air fuel ratio |
| $\lambda_w$ | thermal conductivity |
| $\eta_{Kr}$ | fuel viscosity |
| $\rho_m$ | density of fuel air mixture |
| $\rho_{mm}$ | density on the centerline |
| $\rho_f$ | fuel density |
| $\rho_D$ | fuel density in the droplet |
| $\rho_a$ | air density in cylinder |
| $\sigma_f$ | surface tension of fuel |
| $\omega_D$ | air swirl velocity |

# 11. Appendix 1: Equations

$$2\pi \int_0^{r_j} \frac{y_k}{m_{D,k}} r\, dr = 2\pi \int_0^{r_{jo}} \frac{y_{o,k}}{m_{Do,k}} r\, dr \qquad \left[\frac{\text{Tropfen}}{s}\right] \tag{1}$$

$$r_j^2 \frac{y_{m,k}}{m_{D,k}} = r_{jo}^2 \frac{y_{mo,k}}{m_{Do,k}} \qquad \left[\frac{\text{Tropfen}}{s}\right] \tag{2}$$

$$\frac{\partial}{\partial s}\left( r_j^2 \frac{y_{m,k}}{m_{D,k}} \right) = 0 \tag{3}$$

$$\frac{\partial (m_{D,k})}{\partial t} + \frac{\partial (m_{D,k})}{\partial s} \cdot \frac{ds}{dt} = 0 \tag{4}$$

$$\dot{m}_{Dv,k} = - w_m \frac{\partial (m_{D,k})}{\partial s} \tag{5}$$

$$\frac{\partial}{\partial s}\left( r_j^2\, y_{m,k} \right) = - r_j^2 \frac{y_{m,k}}{m_{D,k}} \frac{m_{vk}}{w_m} \tag{6}$$

$$\dot{m}_v = 2\pi \int_0^{r_1} C\, \rho_m\, w\, r\, dr \tag{7}$$

$$\frac{\partial}{\partial s}\left( 2\pi \int_0^{r_j} C\, \rho_m\, w\, r\, dr \right) = \frac{\partial}{\partial s}\left( \dot{m}_v \right) \tag{8}$$

$$\frac{\partial}{\partial s}\left( C_m\, w_m\, r_j^2 \right) = \frac{1}{2\pi\, \rho_a\, I_{23}} \cdot \frac{\partial}{\partial s}\left( \dot{m}_v \right) \tag{9}$$

$$f_k = 2\pi \int_0^{r_j} \frac{y_k}{m_{D,k}} r\, dr = 2\pi r_j^2 \frac{y_{m,k}}{m_{D,k}} \int_0^1 e^{a \cdot \bar{r}^{\,b}} r\, d\bar{r} \tag{10}$$

$$\frac{\dot{m}_{Dv,k}}{w_m} \qquad \left[ \frac{\text{kg vapor}}{\text{droplet} \cdot s} \cdot \frac{s}{m} = \frac{\text{kg vapor}}{\text{droplet} \cdot m} \right] \tag{11}$$

$$\frac{\partial}{\partial s}\left( \dot{m}_{v,k} \right) = \frac{\dot{m}_{Dv,k}}{w_m} f_k \tag{12}$$

$$\frac{\partial}{\partial s}\left( \dot{m}_{v,k} \right) = 2\pi\, I_{10} \cdot \frac{r_j^2}{w_m} y_{m,k} \frac{\dot{m}_{Dv,k}}{m_{D,k}} \tag{13}$$

$$\frac{\partial}{\partial s}\left( \dot{m}_d \right) = 2\pi \frac{r_j^2}{w_m} \sum_k I_{10} \cdot y_{m,k} \frac{\dot{m}_{Dv,k}}{m_{D,k}} \tag{14}$$

$$\frac{\partial}{\partial s}\left( C_m \cdot w_r \cdot r_j^2 \right) = \frac{r_j^2}{\rho_a\, I_{23}\, w_m} \sum_k I_{10} \cdot y_{m,k} \frac{\dot{m}_{Dv,k}}{m_{D,k}} \tag{15}$$

$$\frac{\partial}{\partial s}\left( 2\pi \int_0^{j} \rho_m\, w\, r\, dr \right) = \frac{\partial}{\partial s}\left( \dot{m}_a \right) + \frac{\partial}{\partial s}\left( \dot{m}_v \right) \tag{16}$$

$$\frac{\partial}{\partial s}\left( \dot{m}_a \right) = 2\pi\, r_j \left( \rho_a \cdot \rho_{mm} \right)^{0.5} \cdot \left( \alpha' \left| w_m - w_a \cos\varphi \right| + \beta' \left| w_a \sin\varphi \right| \right) \tag{17}$$

$$\frac{\partial}{\partial s}\left( w_m \cdot r_j^2 \right) = \frac{1}{2\pi\, \rho_a\, I_{22}} \left( \frac{\partial}{\partial s} \dot{m}_a + \frac{\partial}{\partial s} \dot{m}_v \right) \tag{18}$$

$$\frac{\partial}{\partial s}\left[w_m r_j^2\left(\sum_k l_{12}\cdot y_{m,k} + l_{24}\cdot\rho_a\cdot w_m\right)\cos\beta_x - w_a r_j^2\left(\sum_k l_{12,k}\cdot y_m + l_{22}\cdot\rho_a\cdot w_m\right)\cos\gamma_x\right] =$$

$$= -\frac{1}{2\pi} c_D\ \rho_a\ w_a^2\ r_j\left[\cos\gamma_x - |\cos\varphi|\cdot\cos\beta_x\right]^2\cos\beta_x \qquad (19)$$

$$l_{23} = \int_0^1 \frac{(1-\bar r^{1.5})^3\cdot\bar r}{1 - C_m\cdot(1-\bar r^{1.5})(1-R_f/R_a)}\,d\bar r \qquad l_{10} = \int_0^1 e^{a\cdot\bar r}\cdot\bar r\,d\bar r$$

$$l_{22} = \int_0^1 \frac{(1-\bar r^{1.5})^2\ \bar r}{1 - C_m(1-\bar r^{1.5})(1-R_f'/R_a)}\,d\bar r \qquad l_{12} = \int_0^1 e^{a\cdot\bar r}\cdot(1-\bar r^{1.5})^2\cdot\bar r\cdot d\bar r$$

$$l_{24} = \int_0^1 \frac{(1-\bar r^{1.5})^4\cdot\bar r}{1 - C_m(1-\bar r^{1.5})(1-R_f/R_a)}\,d\bar r \qquad \rho_m = \rho_a\frac{1}{1 - C_m\cdot(1-\bar r^{1.5})(1-R_f/R_a)}$$

$$Q_s = Q_d + Q_v = Q - Q_{\Delta h} \qquad (20)$$

$$Q_s = \alpha_w\ \pi\ d_D^2\,(T - T_D)\,\frac{z}{e^z - 1} \qquad z = \frac{\dot m_{Dv}\cdot c_{pv}}{\alpha_w\,\pi\,d_D^2} \qquad (21)$$

$$\frac{dT_D}{dt} = \frac{2\,\pi\,d_D\,\lambda_W}{(m_{Do} - m_{Dv})\,c_{pD}}\cdot\frac{z}{e^z-1}\,(T - T_D) - \frac{r\cdot\dot m_{Dv}}{(m_{Do} - m_{Dv})\,c_{pD}} \qquad (22)$$

$$-\frac{dm_{Dv}}{dt} = -\dot m_{Dv} = \frac{\pi}{2} d_D^2\,\rho_D\,\frac{d(d_D)}{dt} + \frac{1}{6}\pi\,d_D^3\,\frac{d\rho_D}{dT_D}\,\frac{dT_D}{dt} \qquad (23)$$

$$\frac{dm_{Dv}}{dt} = \frac{2\,\pi\,d_D\,M_f\,p}{8.314\ T_{DA}}\,D_{fa}\,\ln\left(\frac{p}{p - p_v}\right) \qquad (24)$$

$$D = D\left(1 + c\,Re^{0.5}\,Sc^{0.5}\right) \qquad (25\,a) \qquad h = h\left(1 + c\,Re^{0.5}\,Pr^{0.5}\right) \qquad (25\,b)$$

$$m_{SE} = \int_{t_{IA}}^{t_{EE}} \dot m_S\,dt - \int_{t_{IA}}^{t_{EE}} \dot m_{Ox}\,dt \qquad (26)$$

$$\dot m_S = A_S\cdot m_{vf}\cdot p^{0.5}\cdot\exp\left(-\frac{6295}{T}\right) = A_S\cdot m_{vf}\cdot K_S \qquad (27\,a)$$

$$\dot m_{Ox} = A_{Ox}\,\frac{p_{O_2}}{p}\,p^{1.8}\cdot\exp\left(-\frac{7050}{T}\right) = A_{Ox}\,\frac{p_{Ox}}{p}\,K_{Ox} \qquad (27\,b)$$

$$m_{vf} = m_v - m_b \qquad (28)$$

$$f(\omega_{opt}) = 1 + |\omega_{opt} - \omega|^a \qquad (29)$$

$$m_{SE} = \frac{1}{6\cdot n}\left(A_S\cdot m_{vf/ID}\cdot I_S - A_{Ox}\,\frac{\lambda - \lambda_u}{\lambda}\cdot\frac{1}{f(\omega)}\cdot I_{Ox}\right) \qquad (30)$$

$$I_S = \int_{\alpha_{IA}}^{\alpha_{EE}} K_S\,d\alpha \qquad (31\,a) \qquad I_{Ox} = \int_{\alpha_{IA}}^{\alpha_{EE}} K_{Ox}\,d\alpha \qquad (31\,b)$$

$$K_S \sim \frac{m_f\cdot R_{VID}}{n}\cdot\frac{\lambda}{\lambda - \lambda_u}\cdot\frac{I_S}{I_{Ox}}\cdot f(\omega_D) \qquad (32)$$

# 11. Appendix 2: Tables and Figures

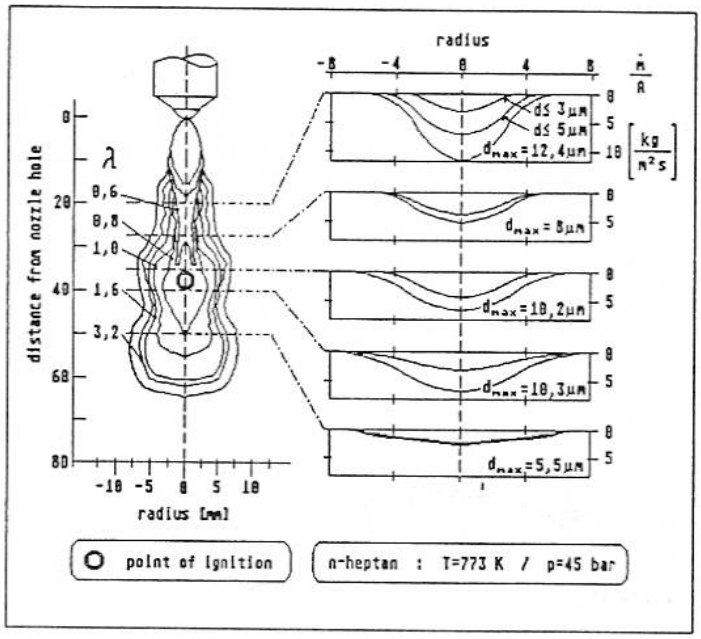


*picture 1* *jet profile, mass flux and maximum diameter in the injection jet [8]*

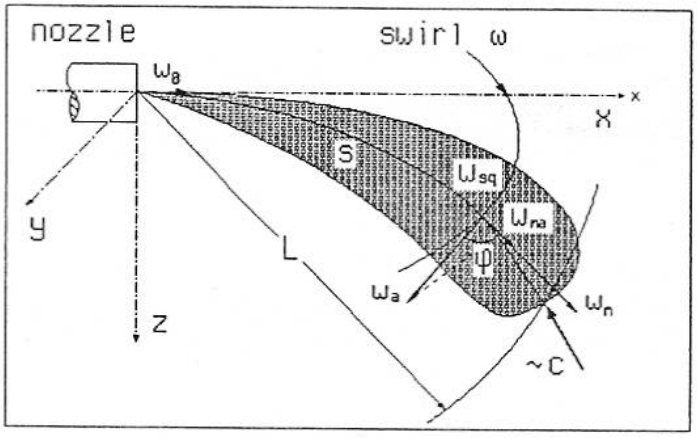


*picture 2* *definitions of the velocities in the injection jet*

| table 1 | data of the both engines used in the tests | |
|---|---|---|
| type | turbocharged | |
| number of cylinders | 6 | 1 |
| cylinder diameter | 128 mm | 128 mm |
| displacement | 11967 $cm^3$ | 1827 $cm^3$ |
| stroke | 155 mm | 142 mm |
| compression ratio | 16.25 : 1 | 17.49 : 1 |
| connecting rod length | 256 mm | 256 mm |

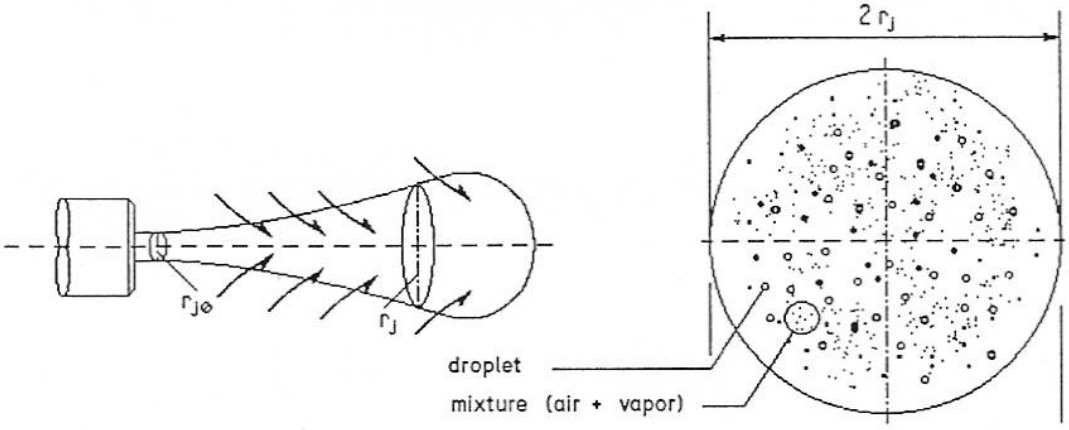


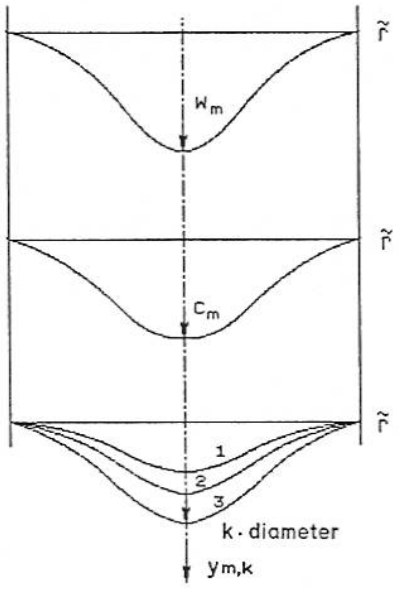


$$w \quad \left[ \frac{m}{s} \right] = w_m \left( 1 - r^{-1.5} \right)^2 \tag{3-1}$$

$$C \quad [ - ] = C_m \left( 1 - r^{-1.5} \right) \tag{3-2}$$

$$\bar{r} = \frac{r}{r_j} \tag{3-3}$$

$$y_k \quad \left[ \frac{kg}{m^2 s} \right] = y_{m,k} \cdot e^{a \cdot r^{-b}} \tag{3-4}$$

$$\frac{y}{m_D} \left[ \frac{kg/m^2\ s}{kg/droplet} = \frac{droplet}{m^2\ s} \right] \tag{3-5}$$

$$d_{Dm} = K_T \frac{d_o^{0.66} \cdot \sigma_f^{0.19} \cdot \eta_f^{0.14}}{\rho_a^{0.26} \cdot \rho_f^{0.07} \cdot w_o^{0.532}} \tag{3-6}$$

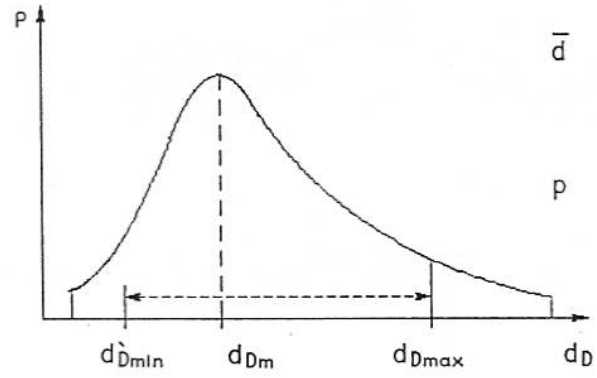


$$\bar{d} = \frac{d_D}{d_{D_{max}}} \tag{3-7}$$

$$p = p_m \cdot e^{a_1 \cdot d^{-b_1}} \tag{3-8}$$

***picture 3*** *velocities, concentrations, mass flux and statistical distribution of droplet diameters in the fuel jet model*

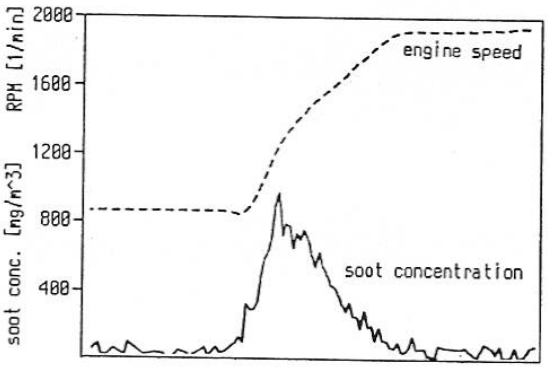


**picture 4 a** *soot concentration and engine speed during acceleration*

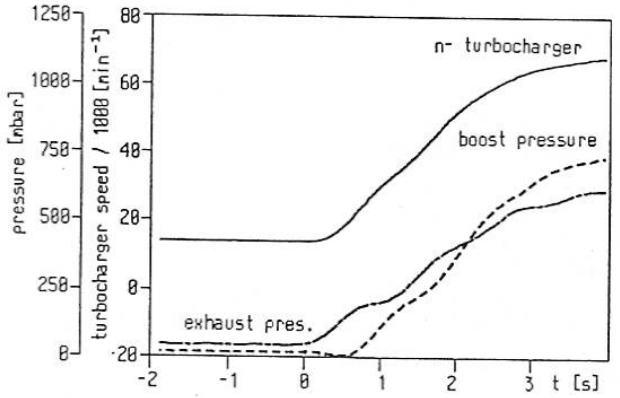


**picture 4 b** *turbocharger speed, boost pressure and pressure in front of the turbine during the acceleration*

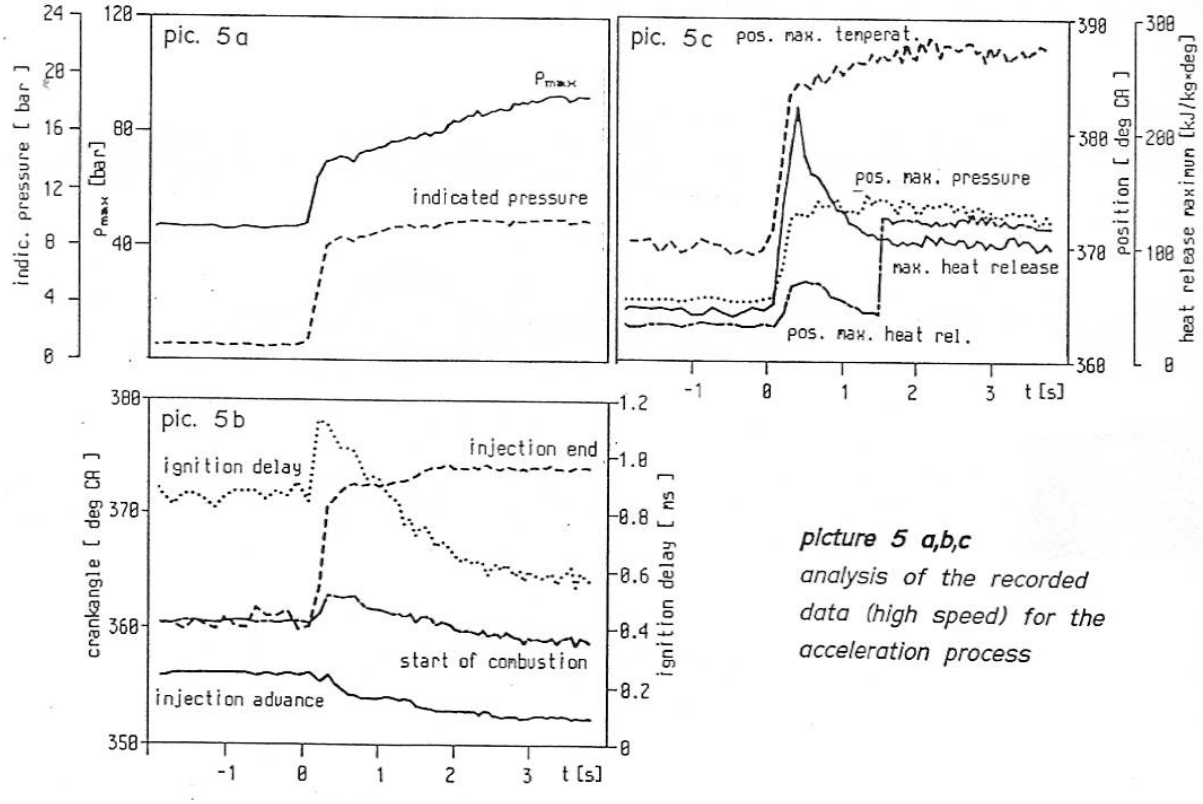


**picture 5 a,b,c** *analysis of the recorded data (high speed) for the acceleration process*

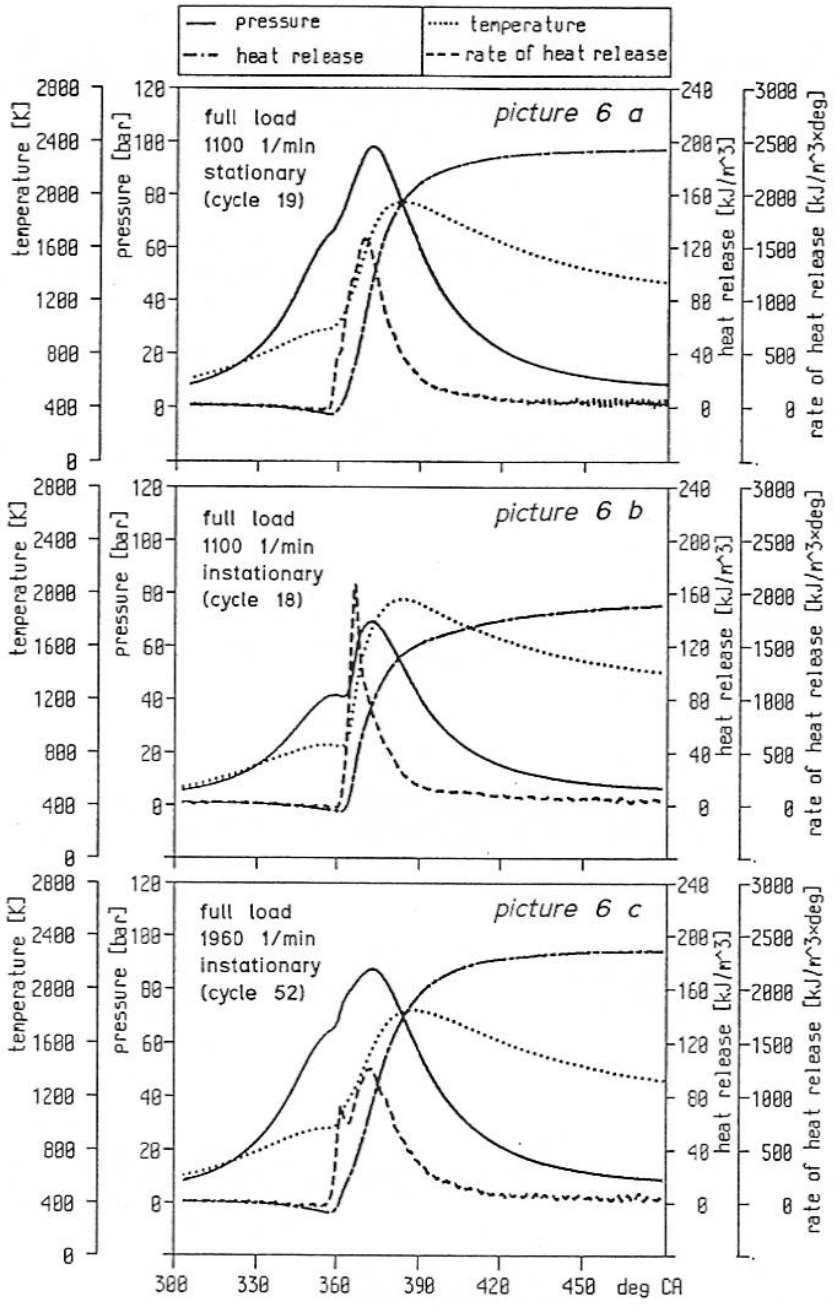


**picture 6** *comparison between stationary and instationary mode pressure, computed temperature and heat release*

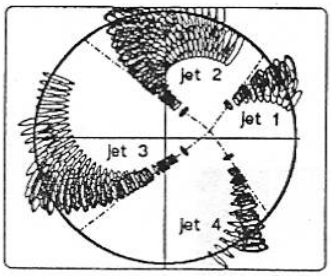


**7a** *jet trajectories full load 1100 1/min stationary*

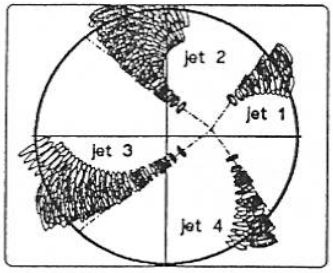


**7b** *jet trajectories full load 1100 1/min instationary*

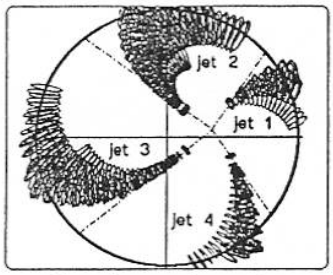


**7c** *jet trajectories full load 1960 1/min instationary*

**picture 7** *fuel jet trajectories*

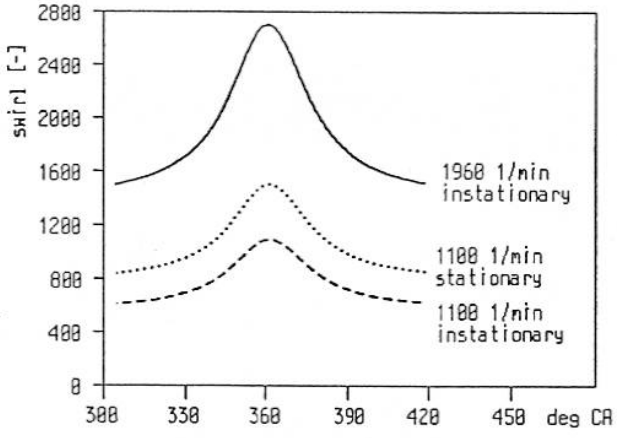


**picture 8** *course of swirl in stationary and instationary mode*

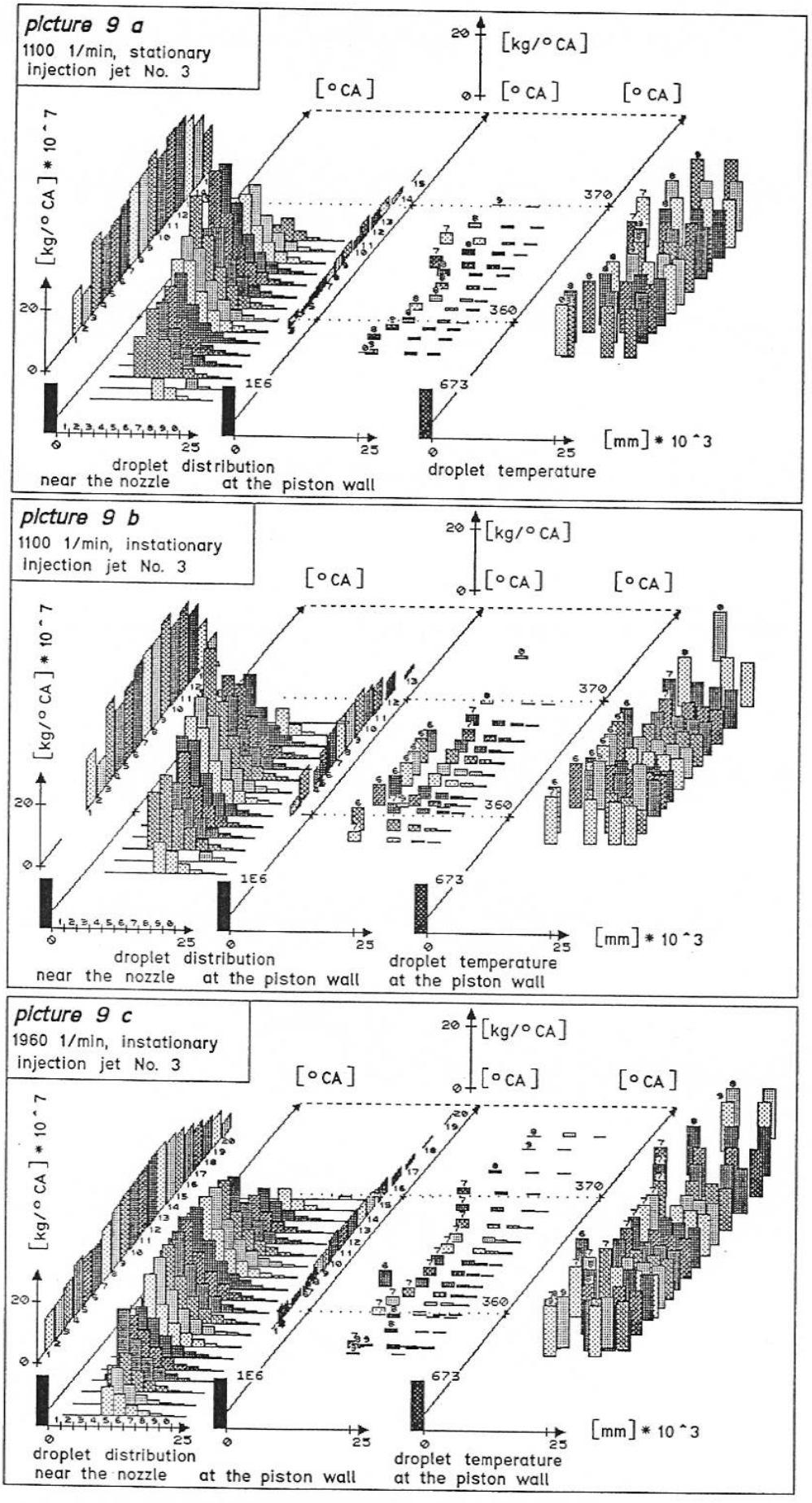


**picture 9** *comparison of the injection jets in stationary and instationary mode*

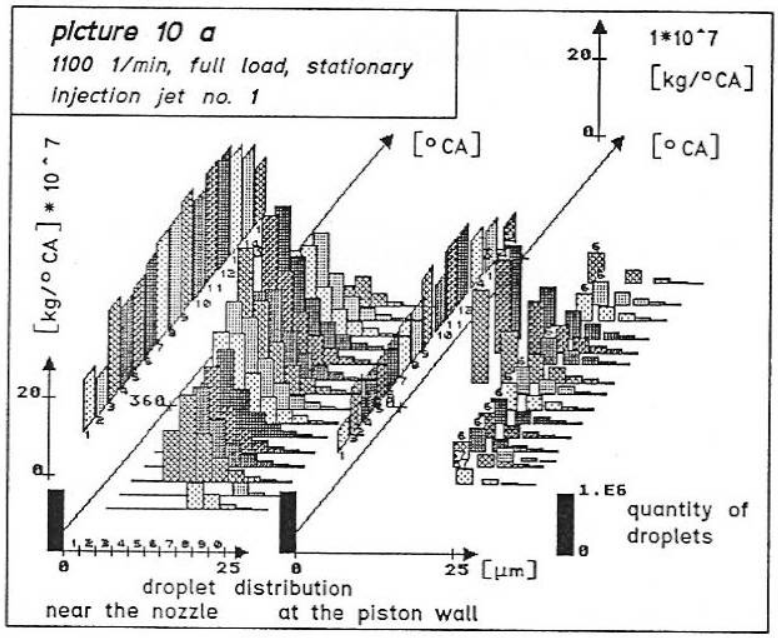


**picture 10** *comparison of long and short injection jets*

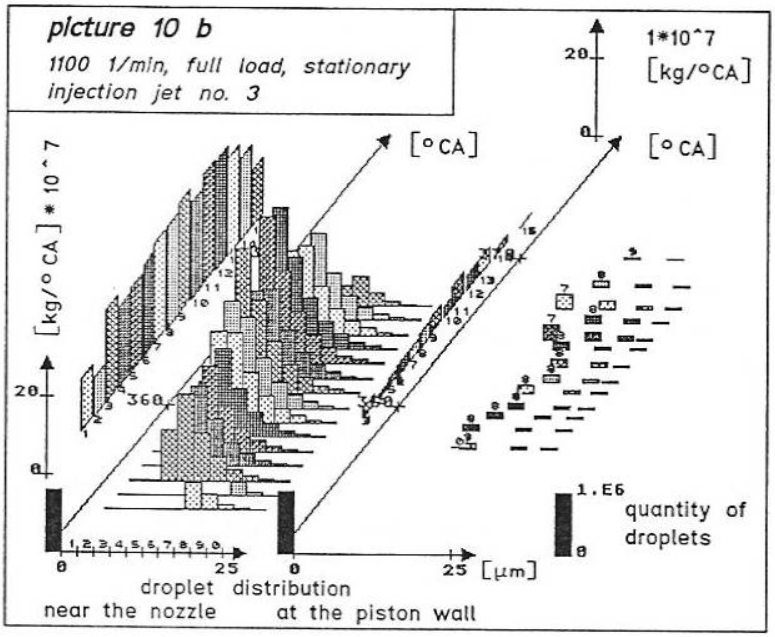


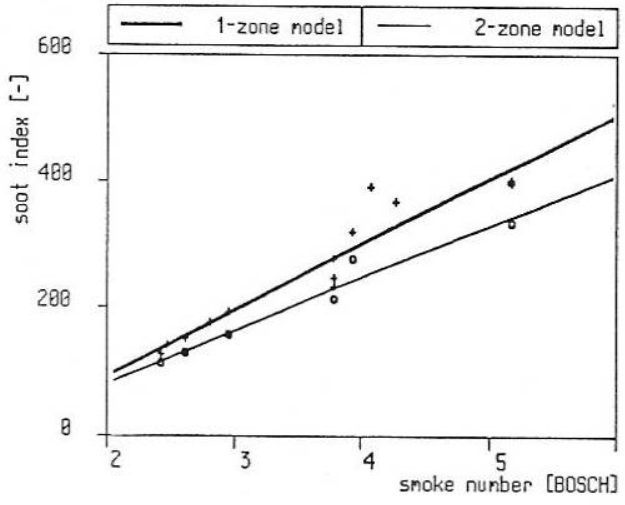


**picture 11** *comparison between soot index and smoke number*

| table 2 a | mean temperature in the injection sections [K] | | | | | | | |
|---|---|---|---|---|---|---|---|---|
| injection section | 1 | 3 | 5 | 7 | 9 | 11 | 13 | 15 |
| injection jet no. 1 | 644 | 584 | 588 | 597 | 580 | 591 | 662 | 668 |
| injection jet no. 2 | *) | 663 | 677 | 676 | 664 | 670 | 682 | 688 |

*) section of injection jet is vaporized before reaching the piston wall

| table 2 b | data of the liquid fuel on the piston wall | | | | |
|---|---|---|---|---|---|
| injection jet number | | 1 | 2 | 3 | 4 |
| mean temperature | [K] | 604 | 673 | 680 | 622 |
| vapor pressure | [bar] | 4.19 | 11.23 | 12.12 | 5.52 |

| table 3 | comparison between smoke number [BOSCH] and soot index | | | | | | |
|---|---|---|---|---|---|---|---|
| cycle (file) | | 1B101 | 1B103 | 1B105 | 1B203 | 1B205 | 1B207 |
| injection advance [° CA] | | 352.5 | 347.8 | 356.5 | 348.1 | 352.0 | 356.4 |
| air-fuel-ratio | $\lambda$ | 1.332 | 1.330 | 1.331 | 1.348 | 1.356 | 1.360 |
| air surplus | $\frac{\lambda}{\lambda - \lambda_u}$ | 2.108 | 2.111 | 2.365 | 2.080 | 2.067 | 2.061 |
| inverse engine speed | $\frac{1}{n}$ | $9.663 * 10^{-4}$ | $9.663 * 10^{-4}$ | $9.663 * 10^{-4}$ | $6.210 * 10^{-4}$ | $6.214 * 10^{-4}$ | $6.210 * 10^{-4}$ |
| relative vapor mass | $R_{VID}$ | 0.215 | 0.191 | 0.221 | 0.228 | 0.209 | 0.194 |
| integral of soot formation reaction (2-zone-model) | $I_S$ | 30.9 | 35.1 | 25.4 | 34.7 | 32.1 | 26.1 |
| integral of soot oxidation reaction (2-zone-model) | $I_{Ox}$ | 4850 | 6380 | 3390 | 6280 | 5170 | 3510 |
| quotient of the both soot functions (2-zone-model) | $\frac{I_S}{I_{Ox}}$ | $6.371 * 10^{-3}$ | $5.502 * 10^{-3}$ | $7.493 * 10^{-3}$ | $5.525 * 10^{-3}$ | $6.209 * 10^{-3}$ | $7.436 * 10^{-3}$ |
| integral of the soot formation reaction (1-zone-model) | $I_S$ | 10.9 | 14.2 | 8.13 | 14.1 | 11.5 | 8.2 |
| integral of the soot oxidation reaction (1-zone-model) | $I_{Ox}$ | 1480 | 2360 | 902 | 2280 | 1584 | 898 |
| quotient of the both soot functions (1-zone-model) | $\frac{I_S}{I_{Ox}}$ | $7.365 * 10^{-3}$ | $6.017 * 10^{-3}$ | $9.013 * 10^{-3}$ | $6.184 * 10^{-3}$ | $7.260 * 10^{-3}$ | $9.131 * 10^{-3}$ |
| fuel mass [mg] | $m_f$ | 98.6 | 98.3 | 98.3 | 98.5 | 98.6 | 98.4 |
| soot index (2-zone-model) | $K_{SE}$ | $275.0 * 10^{-6}$ | $210.7 * 10^{-6}$ | $330.9 * 10^{-6}$ | $113.9 * 10^{-6}$ | $130.4 * 10^{-6}$ | $158.2 * 10^{-6}$ |
| soot index (1-zone-model) | $K_{SE}$ | $318.0 * 10^{-6}$ | $230.4 * 10^{-6}$ | $398.8 * 10^{-6}$ | $127.5 * 10^{-6}$ | $152.9 * 10^{-6}$ | $194.3 * 10^{-6}$ |
| measured soot number [BOSCH] | SZ | 3.95 | 3.8 | 5.2 | 2.4 | 2.6 | 2.95 |